AGU PUBLICATIONS

Geophysical Research Letters

RESEARCH LETTER
10.1002/2017GL072717

Key Points:
- Martian mesospheric clouds are observed by solar scattering of midultraviolet sunlight from a fully illuminated atmosphere
- The early morning mesospheric cloud observations are complementary to previous observations, which are primarily made in the afternoon
- The data suggest that the geographic distribution of clouds is controlled by tides that propagate all the way to the upper atmosphere

Correspondence to:
M. H. Stevens,
michael.stevens@nrl.navy.mil

Citation:
Stevens, M. H., et al. (2017), Martian mesospheric cloud observations by IUVS on MAVEN: Thermal tides coupled to the upper atmosphere, *Geophys. Res. Lett.*, *44*, 4709–4715, doi:10.1002/2017GL072717.

Received 18 JAN 2017
Accepted 4 MAY 2017
Accepted article online 8 MAY 2017
Published online 29 MAY 2017

Martian mesospheric cloud observations by IUVS on MAVEN: Thermal tides coupled to the upper atmosphere

M. H. Stevens[1], D. E. Siskind[1], J. S. Evans[2], S. K. Jain[3], N. M. Schneider[3], J. Deighan[3], A. I. F. Stewart[3], M. Crismani[3], A. Stiepen[4], M. S. Chaffin[3], W. E. McClintock[3], G. M. Holsclaw[3], F. Lefèvre[5], D. Y. Lo[6], J. T. Clarke[7], F. Montmessin[5], and B. M. Jakosky[3]

[1]Space Science Division, Naval Research Laboratory, Washington, District of Columbia, USA, [2]Computational Physics, Inc., Springfield, Virginia, USA, [3]Laboratory for Atmospheric and Space Physics, Boulder, Colorado, USA, [4]Laboratoire de Physique Atmosphérique et Planétaire, Space Sciences, Technologies and Astrophysics Research Institute, Université de Liége, Liége, Belgium, [5]LATMOS, CNRS/UPMC/UVSQ, Paris, France, [6]Lunar and Planetary Laboratory, University of Arizona, Tucson, Arizona, USA, [7]Center for Space Physics, Boston University, Boston, Massachusetts, USA

Abstract We report observations of Martian mesospheric ice clouds and thermospheric scale heights by the Imaging Ultraviolet Spectrograph on NASA's Mars Atmosphere and Volatile Evolution mission. The clouds are observed between 6 A.M. and 8 A.M. local time using mid-UV limb observations between 60 and 80 km tangent altitude where ice particles that scatter sunlight can appear as detached layers near the equator. The equatorial longitudinal distribution shows populations of clouds near −110°E and −10°E as well as a population near 90°E, which does not have a clear precedent. The cloud populations indicate a wave 3 pattern near 70 km, which is confirmed by independent mesospheric temperature observations. Scale heights 100 km above the clouds derived from concurrent Imaging Ultraviolet Spectrograph (IUVS) observations also reveal a wave 3 longitudinal structure, suggesting that the temperature oscillations enabling the formation of mesospheric clouds couple to the upper atmosphere.

Plain Language Summary The manuscript describes the observation of Martian mesospheric clouds between 60 and 80 km altitude by the Imaging Ultraviolet Spectrograph (IUVS) on NASA's MAVEN spacecraft. The cloud observations are uniquely obtained at early morning local times, which complement previous observations obtained primarily later in the diurnal cycle. Differences in the geographic distribution of the clouds from IUVS observations indicate that the local time is crucial for the interpretation of mesospheric cloud formation. We also report concurrent observations of upper atmospheric scale heights near 170 km altitude, which are diagnostic of temperature. These observations suggest that the dynamics enabling the formation of mesospheric clouds propagate all the way to the upper atmosphere.

1. Introduction

Martian mesospheric clouds between 60–80 km altitude were first reported by *Clancy and Sandor* [1998] using Mars Pathfinder camera images obtained from the surface. Although they argued that the clouds were composed of CO_2 ice based on separate temperature observations [*Schofield et al.,* 1997], the first unambiguous identification of Martian mesospheric CO_2 ice was by *Montmessin et al.* [2007] using near-IR imaging spectra. Because average ambient temperatures near 70 km are typically 10–15 K higher than the CO_2 frost point, these clouds are valuable diagnostics for quantifying temperature variability in the Martian mesosphere [*Clancy and Sandor*, 1998].

More recent satellite observations helped to define the seasonal and geographic distributions of mesospheric clouds [e.g., *Clancy et al.,* 2007; *Määttänen et al.,* 2010; *Scholten et al.,* 2010; *Vincendon et al.,* 2011; *Määttänen et al.,* 2013a; *Sefton-Nash et al.,* 2013] such that climatologies could ultimately be compiled [e.g., *Määttänen et al.,* 2013b]. These climatologies revealed that the clouds primarily form near the equator between about 20°S and 20°N distributed between about −130°E and 30°E. In addition to this, there is a seasonal dependence such that the equatorial clouds appear between about L_s = 0–150°, although some observations indicate that the season could start as early as L_s = 330° [*Määttänen et al.,* 2010].

Mid-UV (MUV; 180–340 nm) limb radiances in the Martian mesosphere are relatively bright and often the result of strong Rayleigh scattered sunlight or solar scattering from dust and aerosols. This bright background obscures the identification of ice particles in the upper mesosphere. As a result, very few observations of dust or cloud layers have ever been reported there from MUV solar scattering in a fully illuminated atmosphere [*Rannou et al.,* 2006]. By contrast, solar scattering MUV limb observations of terrestrial mesospheric clouds is a well-established technique [e.g., *Thomas and Olivero*, 1989; *Bailey et al.,* 2005; *Petelina et al.,* 2006; *Stevens et al.,* 2009; *Robert et al.,* 2009].

Here we report solar scattering MUV limb observations of Martian mesospheric ice clouds between 60–80 km from the Imaging Ultraviolet Spectrograph (IUVS) on NASA's Mars Atmosphere and Volatile Evolution (MAVEN) mission. We also report concurrent scale height observations ~100 km higher derived from IUVS dayglow measurements and diagnostic of thermospheric temperatures. We present a possible link between these data sets by using concurrent mesospheric temperature observations from the Mars Climate Sounder (MCS) on the Mars Reconnaissance Orbiter (MRO).

We describe the IUVS observations in section 2 and the spectral analysis as well as cloud identification in section 3. We present the results in section 4, including the complementary IUVS scale height observations. In section 5 we discuss the implications for these results and summarize the findings.

2. The IUVS Limb Observations in the Mesosphere

The IUVS instrument [*McClintock et al.,* 2015] on NASA's MAVEN mission [*Jakosky et al.,* 2015] has been observing the Martian upper atmosphere since October 2014. MAVEN orbits Mars about five times a day and near periapsis IUVS scans the limb using two channels: a MUV channel and a far-UV (110–190 nm) channel. From 13 October through 19 December 2015 (L_s = 54°–83°) IUVS scanned the limb during the mesospheric cloud season, covering all longitudes between 27°N and 72°S latitude. At the lowest tangent altitudes (below 100 km), solar scattered light typically appears in the MUV limb spectra which occasionally includes excess solar scattering from mesospheric ice particles. During this time of year, the contribution to the MUV signal from the Martian haze is very low [*Montmessin et al.,* 2006] so that the excess signal above the Rayleigh background can be interpreted as scattering exclusively from mesospheric ice particles.

The formation of mesospheric CO_2 ice is expected to depend on the local time (LT) of the observations because of the strong migrating diurnal tide on Mars [e.g., *González-Galindo et al.,* 2011]. For our first observations on 13 October the equatorial crossing is ~9 AM LT whereas for the last observations on 19 December it is ~5 AM LT. The scans therefore sample the morning hours just after sunrise, when the temperature minimizes over the diurnal cycle in the upper mesosphere during the cloud season [*Kleinböhl et al.,* 2013]. These early morning data complement the more limited set of morning mesospheric cloud observations reported between 8–11 AM LT from Mars Express by *Määttänen et al.* [2010].

The 0.06° × 11° IUVS field of view is binned into seven horizontal segments (1.6° each) for each of 12 limb scans, allowing for up to 84 separate profiles for analysis each orbit. The vertical resolution of the IUVS data varies depending on which scans are considered, because those at periapsis are closer to the tangent point. Moreover, the IUVS field of view can be tilted a small amount with respect to the horizon [*McClintock et al.,* 2015; *Jain et al.,* 2015], further affecting the resolution. Overall for the data in this study, the vertical resolution varies between 8–17 km in the mesosphere, depending on which scan is analyzed. We use IUVS Level 1b (L1b) calibrated "periapse" limb radiance profiles from the v07 release.

We note here that MAVEN is designed to investigate the upper atmosphere rather than the mesosphere. As a result, the vertical range for each upper atmospheric limb scan varies such that not every scan extends down to 60 km tangent altitude, which is the lowest altitude considered for cloud detection. We furthermore only can use scans for which the solar zenith angle (SZA) is less than 95°. For the 68 days considered, 10,009 limb scans (~50%) extend down to 60 km with SZA $<$ 95° and we focus on these fully illuminated mesospheric scans.

3. Spectral Analysis: Mesospheric Cloud Detection

The detection of mesospheric clouds relies on the brightness of the sunlight scattered from the ice particles. IUVS periapse scans are typically analyzed using a multiple linear regression (MLR) technique that fits the observed limb spectra using the spectral shape of known Martian UV emissions [*Stevens et al.,* 2015;

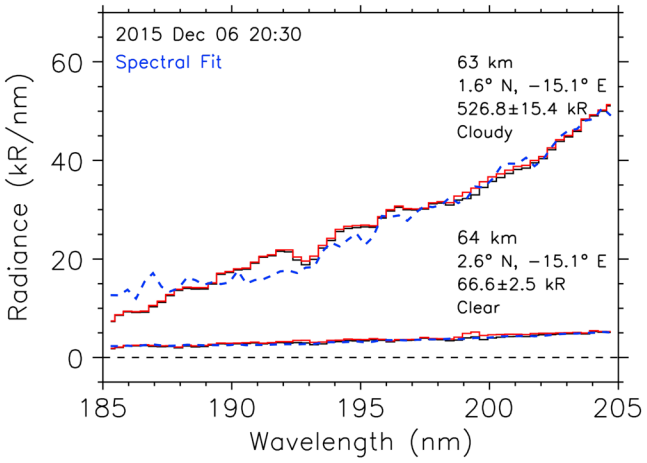

Figure 1. Limb spectra from IUVS scans between 63 and 64 km tangent altitude. The observed spectra (red histogram) include a small contribution (~10 kR) from the CO Cameron bands. The solar scattered contribution is overplotted (black histogram) along with the spectral fit (blue dashed). The two observations are separated by 60 km at the tangent point. The indicated radiance is calculated by integrating over the passband shown.

Schneider et al., 2015a; *Schneider et al.,* 2015b; *Evans et al.,* 2015; *Jain et al.,* 2015; *Lo et al.,* 2015]. The shape of the prominently bright CO_2^+ Ultraviolet Doublet (UVD) near 289 nm is used to determine the IUVS MUV wavelength registration for each orbit.

For the detection of mesospheric clouds, the IUVS operational algorithm is modified so that only the CO Cameron band system [e.g., *Stevens et al.,* 2015] and the solar spectral shape are included in the fit. As we will show, the spectral shape of the signal from mesospheric ice particles or Rayleigh scattered light resemble the solar spectrum over the spectral region used for the retrieval. We use a single IUVS observation of backscattered sunlight from the Martian disk as a template for the solar spectral shape. For the tangent altitudes of interest here, the solar scattered contribution can be so bright that it saturates the detector. We therefore only fit the spectral region between 185–205 nm, which is at long enough wavelengths to yield a detectable solar scattered signal but at short enough wavelengths to avoid saturation. At these wavelengths only the solar scattered light contributes significantly to the limb spectra, with only a small contribution from the CO Cameron bands. The varying IUVS spectral binning is accounted for in the fitting.

Figure 1 shows IUVS limb spectra near 63 km tangent altitude for two different parts of the IUVS aperture from a scan on 6 December 2015. The tangent altitudes are at the same longitudes and 1.0° (60 km) apart in latitude. One spectrum is about eight times brighter than the other, indicating the presence of a mesospheric cloud along the line of sight. Both spectral fits are good and demonstrate the reliability of the approach for detecting solar scattered light in the Martian mesosphere, either with or without a mesospheric cloud present. Figure 2 shows the radiance profiles associated with the two limb spectra in Figure 1 and the mesospheric cloud detection is well above the measurement uncertainty.

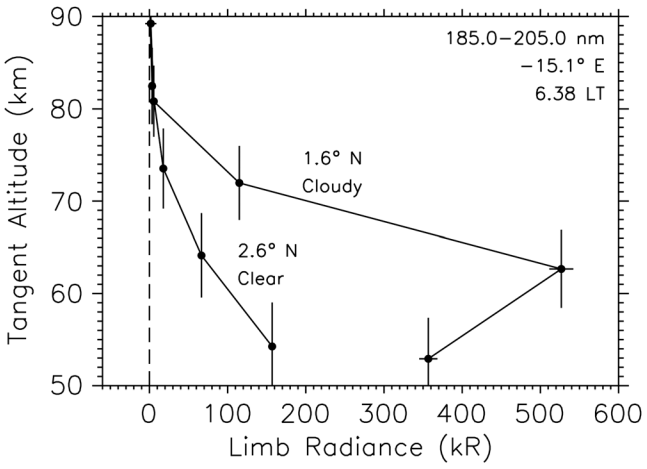

Figure 2. Limb radiance profiles associated with the spectra shown in Figure 1. The statistical uncertainties (horizontal lines) are those returned from the MLR, and the vertical lines associated with each spectrum represent the vertical resolution of the measurements.

Figure 3 shows the radiance profiles of the solar scattered component for all identified cloud scans. An average radiance as well as a standard deviation (σ) is calculated at each altitude based on the observed scatter of measurements and we choose a 5σ threshold to identify mesospheric clouds. The 5σ threshold is chosen subjectively and conservatively to be high enough to ensure no false detections and is the same as that used for early studies of terrestrial mesospheric clouds [*Thomas and Olivero*, 1989]. Using this threshold, we initially identify 91 mesospheric clouds in the complete data set. However, in order to reduce the positive bias on the threshold due to the brightest clouds, we iterate once more after removing

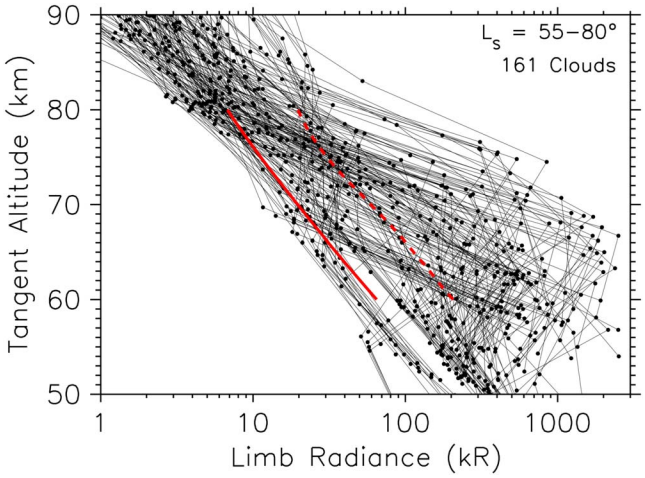

Figure 3. Mesospheric profiles of solar scattered radiance for all mesospheric cloud scans identified in this study. The average of all IUVS profiles is shown (solid red, see text), and the 5σ threshold calculated from the scatter at each altitude is overplotted (dashed red).

these 91 scans with clouds identified. On the next iteration, we identify 70 more scans with clouds for a total of 161. Another iteration does not yield any more cloud detections. Many of the identified scans in Figure 3 (90 or 56%) show a detached cloud layer between 60–80 km, for which the average peak altitude is 67.5 km. Those clouds not identified as detached may nonetheless be so because the IUVS vertical resolution of 8–17 km may not be high enough to resolve the separation from the background signal. Figure 3 nonetheless shows that there is an unambiguous difference between the average clear air profile and those containing clouds.

4. Results: Coupling to the Upper Atmosphere

We assemble the cloud detections geographically in Figure 4. There is a population of clouds near 45°S and 160°E, which has been observed before during this season although much later in the day near 3 PM LT [*Sefton-Nash et al.,* 2013]. However, in this study we concentrate on the large number of clouds in a narrow ±20° latitude band around the equator. The equatorial clouds cluster in geographic longitude such that many are near −110°E and −10°E, consistent with previous observations [*Clancy et al.,* 2007; *Määttänen et al.,* 2010; *McConnochie et al.,* 2010; *Vincendon et al.,* 2011]. A third equatorial population is detected near 90°E, which does not have a clear precedent. The IUVS equatorial cloud observations were made from 6 AM to 8 AM LT, which is much earlier in the day than most of the previous observations. Although OMEGA observed some equatorial clouds from 8 to 11 AM LT [*Määttänen et al.,* 2010], most others reported to date were observed from 1 PM to 6 PM LT [*Clancy et al.,* 2007; *Määttänen et al.,* 2010: *Sefton-Nash et al.,* 2013].

During the IUVS mesospheric cloud observations, MCS was measuring mesospheric temperatures [*McCleese et al.,* 2007; *Zurek and Smrekar*, 2007; *Kleinböhl et al.,* 2009] early in the morning near the equator. Figure 5a shows MCS temperatures as a function of longitude at 75 km. The temperature minima in Figure 5a are at similar longitudes as the concurrent IUVS equatorial cloud observations in Figure 4, even though the MCS observations are 2–3 h in LT prior to the IUVS cloud observations. Indeed, the small difference in LT between the two data sets may help explain why the IUVS cloud observations do not precisely align with the MCS temperature minima. Figure 5a also shows the CO_2 frost point [*Meyers and Van Dusen*, 1933] calculated from the same MCS observations. The frost points show that additional downward temperature excursions of 20–30 K are required to enable mesospheric cloud formation.

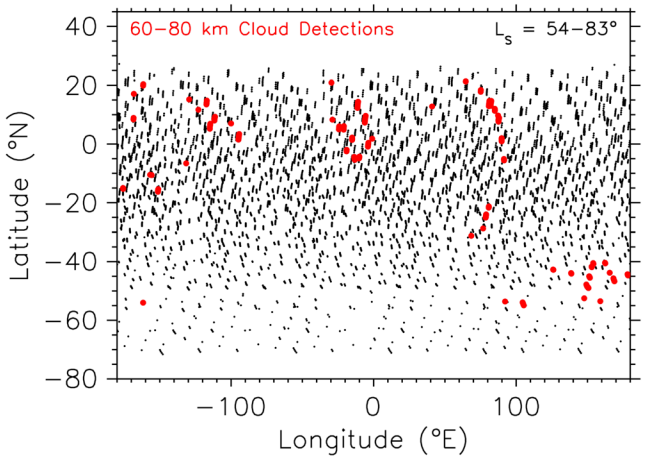

Figure 4. The geographic distribution of all the mesospheric limb scans used in this work. The cloud observations from Figure 3 (L_s = 55°–80°) are overplotted in red and show three groups near the equator, which are observed between 6 A.M. and 8 A.M. LT.

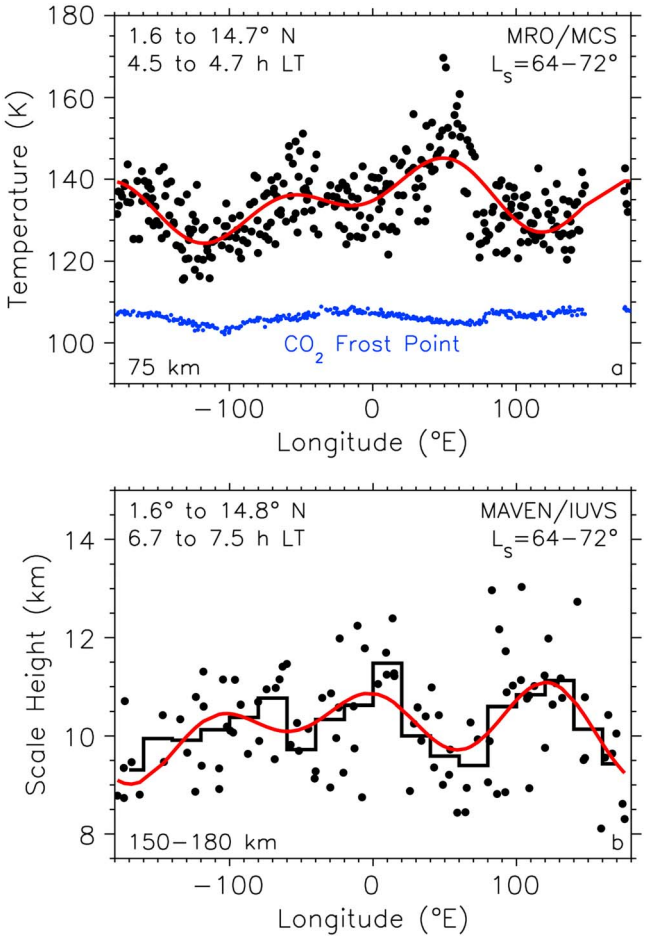

Figure 5. (a) MRO/MCS temperature observations at 75 km altitude between 6 and 23 November 2015 for the indicated latitudes and LT (black dots). Statistical uncertainties for each measurement are 11 K on average. The red solid line is a harmonic fit to the data, showing a strong wave 3 component (see text). The equatorial IUVS mesospheric clouds are observed near the MCS temperature minima (cf. Figure 4). The CO_2 frost points calculated from the MCS temperatures are overplotted in blue. (b) MAVEN/IUVS thermospheric scale heights (black dots) derived for the same time period as the MCS temperatures in Figure 5a. LT are 2–3 h after the MCS observations. The black histogram is an average over 20° bins, suggesting a strong wave 3 component. The red solid line is a harmonic fit to all the data.

Identifying the source of this additional variability is beyond the scope of this work but may be related to local gravity wave activity [e.g., *Spiga et al.,* 2012; *Yiğit et al.,* 2015].

Following the approach of *Lo et al.* [2015] who reported the observation of nonmigrating tides in the Martian upper atmosphere, we fit the equatorial temperature data in Figure 5a with a series of harmonics. We assume that the observations are fixed in LT and fit the tidal components in a least squares sense using the function

$$T(\lambda) = T_0 + A_k \cos(k\lambda - \delta_k) \quad (1)$$

where λ is longitude, T_0 is the average temperature, A_k is the amplitude of wave component k, δ is the phase of component k, and k = 1, 2, or 3 represent the wave 1, 2, or 3 contributions. The best fit solution to the fit is overplotted in Figure 5a, where the wave 3 amplitude is the largest (A_3 = 5.6 K), followed by the wave 1 amplitude (A_1 = 4.5 K), and the wave 2 amplitude (A_2 = 3.2 K).

Based upon previous observations and model results [e.g., *Bougher et al.,* 1993; *Forbes et al.,* 2002; *Withers et al.,* 2003; *Kleinböhl et al.,* 2013; *Moudden and Forbes*, 2014; *Medvedev et al.*, 2016; *Liu et al.,* 2017], it is plausible to expect that the temperature perturbations affecting the mesosphere propagate to the upper atmosphere. IUVS measures the scale heights in the upper atmosphere from radiance profiles of the CO_2^+ Ultraviolet Doublet [*Lo et al.,* 2015], which are diagnostic of temperature variations between 150 and 180 km [*Bougher et al.,* 2017]. These results are shown in Figure 5b for the same L_s as the MCS observations in Figure 5a. To reduce the scatter of the data, we include an average over 20° longitudinal bins, which suggests a strong wave 3 contribution. A fit using equation (1) reveals that wave 3 is the strongest component (5%), followed by wave 2 (4%), and wave 1 (3%). The wave 3 contribution is therefore prominent in both the thermosphere [*Liu et al.,* 2017] and mesosphere. We expect the relative contributions of these components to vary with LT and latitude [*England et al.,* 2016].

We note that the wave 3 IUVS scale height oscillations are nearly anticorrelated with the MCS mesospheric temperature oscillations. The quantitative relationship between the thermospheric and the mesospheric wave 3 structure requires additional information on the vertical wavelength, the phase, and the amplitude variation of the oscillation with altitude and LT [e.g., *Määttänen et al.,* 2010], which is beyond the scope of this work. Nevertheless, Figures 4 and 5 together provide a strong suggestion that the oscillations enabling mesospheric cloud formation concurrently propagate all the way to the thermosphere.

5. Summary

We report the observation of Martian mesospheric clouds between 60 and 80 km from MUV daytime limb scans by IUVS on MAVEN. The cloud observations were made in 2015 between spring equinox and summer solstice in the Northern Hemisphere (L_s = 55°-80°). The latitudinal distribution of the clouds is consistent with previous mesospheric cloud observations, with many of them detected near the equator. Longitudinal clustering of the equatorial clouds near −110°E and −10°E is also consistent with previous observations, although we report an additional population near 90°E. This longitudinal distribution indicates a strong wave 3 component, generally consistent with MCS mesospheric temperature observations during the same time period.

We also report IUVS-derived scale heights ~100 km higher and concurrent with the cloud observations. These data also show that a wave 3 component is strong, but roughly 180° out of phase with the mesospheric temperature observations. This suggests that the same tidal variability enabling cloud formation between 60 and 80 km propagates to altitudes 100 km higher. The IUVS mesospheric cloud and scale height observations together show that the clouds reflect changes throughout the atmosphere and provide new constraints to general circulation models.

Acknowledgments
The MAVEN project is supported by NASA through the Mars Exploration Program. M.H.S. and D.E.S. were supported by the NASA MAVEN Participating Scientist program. The IUVS cloud observations and scale height data presented in this work are available on the MAVEN Science Data Center (SDC) website at LASP (https://lasp.colorado.edu/maven/sdc/public/). The IUVS L1b data and the MCS temperature data are available on the Planetary Data System (PDS). We thank David Kass for guidance on the MCS data set and for several discussions from which this work benefited. We also thank two anonymous reviewers who made many constructive suggestions that substantially improved the manuscript.

References

Bailey, S. M., A. W. Merkel, G. E. Thomas, and J. N. Carstens (2005), Observations of polar mesospheric clouds by the Student Nitric Oxide Explorer, *J. Geophys. Res.*, *110*, D13203, doi:10.1029/2004JD005422.

Bougher, S. W., C. G. Fesen, E. C. Ridley, and R. W. Zurek (1993), Mars mesosphere and thermosphere coupling: Semidiurnal tides, *J. Geophys. Res.*, *98*, 3281–3295.

Bougher, S. W., et al. (2017), The structure and variability of Mars dayside thermosphere from MAVEN NGIMS and IUVS measurements: Seasonal and solar activity trends in scale heights and temperatures, *J. Geophys. Res. Space Physics*, *122*, 1296–1313, doi:10.1002/2016JA023454.

Clancy, R. T., and B. J. Sandor (1998), CO_2 ice clouds in the upper atmosphere of Mars, *Geophys. Res. Lett.*, *25*, 489–492.

Clancy, R. T., M. J. Wolff, B. A. Whitney, B. A. Cantor, and M. D. Smith (2007), Mars equatorial mesospheric clouds: Global occurrence and physical properties from Mars Global Surveyor Thermal Emission Spectrometer and Mars orbiter camera limb observations, *J. Geophys. Res.*, *112*, E04004, doi:10.1029/2006JE002805.

England, S. L., et al. (2016), Simultaneous observations of atmospheric tides from combined in situ and remote observations at Mars from the MAVEN spacecraft, *J. Geophys. Res. Planets*, *121*, 594–607, doi:10.1002/2016JE004997.

Evans, J. S., et al. (2015), Retrieval of CO_2 and N_2 in the Martian thermosphere using dayglow observations by IUVS on MAVEN, *Geophys. Res. Lett.*, *42*, 9040–9049, doi:10.1002/2015GL065489.

Forbes, J. M., et al. (2002), Nonmigrating tides in the thermosphere of Mars, *J. Geophys. Res.*, *107*(E11), 5113, doi:10.1029/2001JE001582.

González-Galindo, F., A. Määttänen, F. Forget, and A. Spiga (2011), The Martian mesosphere as revealed by CO_2 cloud observations and general circulation modeling, *Icarus*, *216*, 10–22.

Jain, S. K., et al. (2015), The structure and variability of Mars upper atmosphere as seen in MAVEN/IUVS dayglow observations, *Geophys. Res. Lett.*, *42*, 9023–9030, doi:10.1002/2015GL065419.

Jakosky, B. M., et al. (2015), The Mars Atmosphere and Volatile EvolutioN (MAVEN) mission, *Space Sci. Rev.*, *195*, 3–48, doi:10.1007/s11214-015-0139-x.

Kleinböhl, A., et al. (2009), Mars Climate Sounder limb profile retrieval of atmospheric temperature, pressure, and dust and water ice opacity, *J. Geophys. Res.*, *114*, E10006, doi:10.1029/2009JE003358.

Kleinböhl, A., R. J. Wilson, D. Kass, J. T. Schofield, and D. J. McCleese (2013), The semidiurnal tide in the middle atmosphere of Mars, *Geophys. Res. Lett.*, *40*, 1952–1959, doi:10.1002/grl.50497.

Liu, G., S. England, R. J. Lillis, P. R. Mahaffy, M. Elrod, M. Benna, and B. Jakosky (2017), Longitudinal structures in Mars' upper atmosphere as observed by MAVEN/NGIMS, *J. Geophys. Res. Space Physics*, *122*, 1258–1268, doi:10.1002/2016JA023455.

Lo, D. Y., et al. (2015), Nonmigrating tides in the Martian atmosphere as observed by MAVEN IUVS, *Geophys. Res. Lett.*, *42*, 9057–9063, doi:10.1002/2015GL066268.

Määttänen, A., et al. (2010), Mapping the mesospheric CO_2 clouds on Mars: Mex/OMEGA and Mex/HRSC observations and challenges for atmospheric models, *Icarus*, *209*, 452–469.

Määttänen, A., et al. (2013a), A complete climatology of the aerosol vertical distribution on Mars from Mex/SPICAM UV solar occultations, *Icarus*, *223*, 892–941.

Määttänen, A., K. Perot, F. Montmessin and A. Hauchecorne (2013b), Mesospheric clouds on Mars and on Earth, in *Comparative Climatology of Terrestrial Planets*, edited by S. J. Mackwell et al., pp. 393–413, Univ. of Arizona, Tucson, doi:10.2458/azu_uapress_9780816530595-ch16.

McCleese, D. J., et al. (2007), Mars Climate Sounder: An investigation of thermal and water vapor structure, dust and condensate distributions in the atmosphere, and energy balance of the polar regions, *J. Geophys. Res.*, *112*, E05506, doi:10.1029/2006JE002790.

McClintock, W. E., et al. (2015), The imaging ultraviolet Spectrograph (IUVS) for the MAVEN mission, *Space Sci. Rev.*, *195*, 75–124, doi:10.1007/s11214-014-0098-7.

McConnochie, T. H., et al. (2010), THEMIS-VIS observations of clouds in the Martian mesosphere: Altitudes, wind speeds, and decameter-scale morphology, *Icarus*, *210*, 545–565.

Medvedev, A. S., et al. (2016), Comparison of the Martian thermospheric density and temperature from IUVS/MAVEN data and general circulation modeling, *Geophys. Res. Lett.*, *43*, doi:10.1002/2016GL068388.

Meyers, C. H., and M. S. Van Dusen (1933), The vapor pressure of liquid and solid carbon dioxide, *Bureau of Standards J. Res.*, *10*, 381–412.

Montmessin, F., et al. (2006), Stellar occultations at UV wavelengths by the SPICAM instrument: Retrieval and analysis of Martian haze profiles, *J. Geophys. Res.*, *111*, E09S09, doi:10.1029/2005JE002662.

Montmessin, F., et al. (2007), Hyperspectral imaging of convective CO_2 ice clouds in the equatorial mesosphere of Mars, *J. Geophys. Res.*, *112*, E11S90, doi:10.1029/2007JE002944.
Moudden, Y., and J. M. Forbes (2014), Insight into the seasonal asymmetry of nonmigrating tides on Mars, *Geophys. Res. Lett.*, *41*, 2631–2636, doi:10.1002/2014GL059535.
Petelina, S. V., E. J. Llewellyn, D. A. Degenstein, and N. D. Lloyd (2006), Odin/OSIRIS limb observations of polar mesospheric clouds in 2001–2003, *J. Atmos. Sol. Terr. Phys.*, *68*, 42–55.
Rannou, P., S. Perrier, J.-L. Bertaux, F. Montmessin, O. Korablev, and A. Rébérac (2006), Dust and cloud detection at the Mars limb with UV scattered sunlight with SPICAM, *J. Geophys. Res.*, *111*, E09S10, doi:10.1029/2006JE002693.
Robert, C. E., C. von Savigny, J. P. Burrows, and G. Baumgarten (2009), Climatology of noctilucent cloud radii and occurrence frequency using SCIAMACHY, *J. Atmos. Sol. Terr. Phys.*, *71*, 408–423.
Schneider, N. M., et al. (2015a), MAVEN IUVS observations of the aftermath of the comet siding spring meteor shower on Mars, *Geophys. Res. Lett.*, *42*, 4755–4761, doi:10.1002/2015GL063863.
Schneider, N. M., et al. (2015b), Discovery of diffuse aurora on Mars, *Science*, *350*, aad0313.
Schofield, J. T., et al. (1997), The Mars Pathfinder Atmospheric Structure Investigation/Meteorology (ASI/MET) experiment, *Science*, *278*, 1752–1757.
Scholten, F., et al. (2010), Concatenation of HRSC colour and OMEGA data for the determination and 3D-parameterization of high-altitude CO_2 clouds in the Martian atmosphere, *Planet. Space Sci.*, *58*, 1207–1214.
Sefton-Nash, E., et al. (2013), Climatology and first-order composition estimates of mesospheric clouds from Mars Climate Sounder limb spectra, *Icarus*, *22*, 342–356.
Spiga, A., F. González-Galindo, M.-Á. López-Valverde, and F. Forget (2012), Gravity waves, cold pockets and CO_2 clouds in the Martian mesosphere, *Geophys. Res. Lett.*, *39*, L02201, doi:10.1029/2011GL050343.
Stevens, M. H., et al. (2009), The diurnal variation of polar mesospheric cloud frequency near 55°N observed by SHIMMER, *J. Atmos. Sol. Terr. Phys.*, *71*, 401–407.
Stevens, M. H., et al. (2015), New observations of molecular nitrogen in the Martian upper atmosphere by IUVS on MAVEN, *Geophys. Res. Lett.*, *42*, 9050–9056, doi:10.1002/2015GL065319.
Thomas, G. E., and J. J. Olivero (1989), Climatology of polar mesospheric clouds 2. Further analysis of solar mesosphere Explorer data, *J. Geophys. Res.*, *94*, 14,693–14,681.
Vincendon, M., C. Pilorget, B. Gondet, S. Murchie, and J.-P. Bibring (2011), New near-IR observations of mesospheric CO_2 and H_2O clouds on Mars, *J. Geophys. Res.*, *116*, E00J02, doi:10.1029/2011JE003827.
Withers, P., S. W. Bougher, and G. M. Keating (2003), The effects of topographically-controlled thermal tides in the Martian upper atmosphere as seen by the MGS accelerometer, *Icarus*, *164*, 14–32.
Yiğit, E., A. S. Medvedev, and P. Hartogh (2015), Gravity waves and high-altitude CO_2 ice cloud formation in the Martian atmosphere, *Geophys. Res. Lett.*, *42*, 4294–4300, doi:10.1002/2015GL064275.
Zurek, R. W., and S. E. Smrekar (2007), An overview of the Mars Reconnaissance Orbiter (MRO) science mission, *J. Geophys. Res.*, *112*, E05501, doi:10.1029/2006JE002701.